The Journal of Experimental Biology 214, 1194-1204
© 2011. Published by The Company of Biologists Ltd
doi:10.1242/jeb.051029

RESEARCH ARTICLE

Scaling of caterpillar body properties and its biomechanical implications for the use of a hydrostatic skeleton

Huai-Ti Lin[1,*], Daniel J. Slate[1], Christopher R. Paetsch[2], A. Luis Dorfmann[2] and Barry A. Trimmer[1]

[1]Department of Biology, Tufts University, 165 Packard Avenue, Dana Lab, Medford, MA 02155, USA and [2]Department of Civil & Environmental Engineering, Tufts University, 200 College Avenue, Anderson Hall, Medford, MA 02155, USA

*Author for correspondence (huai-ti.lin@tufts.edu)

Accepted 6 December 2010

SUMMARY

Caterpillars can increase their body mass 10,000-fold in 2 weeks. It is therefore remarkable that most caterpillars appear to maintain the same locomotion kinematics throughout their entire larval stage. This study examined how the body properties of a caterpillar might change to accommodate such dramatic changes in body load. Using *Manduca sexta* as a model system, we measured changes in body volume, tissue density and baseline body pressure, and the dimensions of load-bearing tissues (the cuticle and muscles) over a body mass range from milligrams to several grams. All *Manduca* biometrics relevant to the hydrostatic skeleton scaled allometrically but close to the isometric predictions. Body density and pressure were almost constant. We next investigated the effects of scaling on the bending stiffness of the caterpillar hydrostatic skeleton. The anisotropic non-linear mechanical response of *Manduca* muscles and soft cuticle has previously been quantified and modeled with constitutive equations. Using biometric data and these material laws, we constructed finite element models to simulate a hydrostatic skeleton under different conditions. The results show that increasing the internal pressure leads to a non-linear increase in bending stiffness. Increasing the body size results in a decrease in the normalized bending stiffness. Muscle activation can double this stiffness in the physiological pressure range, but thickening the cuticle or increasing the muscle area reduces the structural stiffness. These non-linear effects may dictate the effectiveness of a hydrostatic skeleton at different sizes. Given the shared anatomy and size variation in Lepidoptera larvae, these mechanical scaling constraints may implicate the diverse locomotion strategies in different species.

Key words: *Manduca sexta* caterpillar, hydrostatic skeleton, biomechanics of scaling, larval ontogeny, finite element analysis, crawling, inching.

INTRODUCTION

Biomechanical scaling of caterpillars

Typically, in terrestrial animals with rigid skeletons and constant bone density, the cross-sectional area of the skeleton scales disproportionally relative to the representative linear dimension as the body increases in size. This characteristic helps support the increasing body mass and resists the accompanying forces of locomotion, which scale roughly with body volume (Demetrius, 2006; Prange et al., 1979; West et al., 1997).

Mechanical scaling in soft-bodied animals is different because soft tissues undergo very large deformations and increased rigidity can only be achieved through pressurization. Rather than relying on increasing the amount of skeletal material, soft animals can employ hydrostatics to resist the increase in forces associated with locomotion. A true hydrostat, such as the earthworm, can scale isometrically over many orders of magnitude while maintaining a similar static body stress (Quillin, 1998; Quillin, 1999). Leeches also move similarly at all body sizes (Jordan, 1998). Numerous geometric models of hydrostats based on a constant body volume assumption capture the kinematics and dynamics of annelid locomotion (Dobrolyubov and Douchy, 2002; Skierczynski et al., 1996). In locomotor modes with a more complex substrate interaction, body loading depends greatly on body size (Quillin, 2000). During burrowing, for example, behavioral and morphological adaptations are necessary in order to operate at different scales (Che and Dorgan, 2010). Studying the scaling of hydrostatic skeletons helps us understand how a soft-bodied animal copes with mechanical loads at different body sizes.

Soft animals do not all have the same body structure, and for some the maintenance of a pressurized fluid cavity is limited by physiological and mechanical factors. Caterpillars, for example, deviate from the existing constant-volume worm models because they contain air. While worms breathe through their skin, caterpillars have a waxy external body surface to minimize water loss and an extensive internal system of gas-filled tubes (trachea) to facilitate gas exchange (Kramer and Wigglesworth, 1950; Locke, 1997; Wasserthal, 1996). It has been shown behaviorally that gas inside the trachea can be compressed and expelled from the spiracles during locomotion (H.T.L., personal observation). Some caterpillars even exploit this air expulsion mechanism to produce predator startle whistles (Bura et al., 2011). This air leak could compromise the efficiency of the hydrostatic skeleton. Instead of relying on a stiff hydrostatic structure, ground reaction forces of *Manduca* suggest that crawling caterpillars can use the substrate for force transmission (an 'environmental skeleton') during normal locomotion (Lin and Trimmer, 2010). In contrast, inchworms lift most of their body every stride and must be stiff enough to support elevated body positions. This difference suggests that the use of hydrostatic skeletons could

be fundamentally different between animals that employ crawling as their primary form of locomotion and animals that employ an inching gait.

Adding to the complexity of caterpillar body mechanics, there is a developmental shift in the relative proportion of various tissues as the animals grow. First instar hatchlings sink in water but fifth instar *Manduca* caterpillars float, suggesting a change in body density. Unlike vertebrates, which tend to display isometric scaling of lung volume relative to body mass (West et al., 1997), many insects increase their mass-specific tracheation across instars to maintain sufficient oxygen intake (Lease et al., 2006). Although fast growing caterpillars such as *Manduca sexta* decrease their gas exchange capacity as they grow (Greenlee and Harrison, 2005), a decrease in body density could be through a change in tissue composition, for example through the accumulation of fat tissues (Fernando-Warnakulasuriya et al., 1988; Tsuchida and Wells, 1988).

In this study, we investigated the effects of different body properties (such as body size, tissue cross-sectional area and the state of muscle activation) on the overall bending stiffness of the internal hydrostatic skeleton in caterpillars. Although *Manduca* can crawl using a tension-based strategy (Lin and Trimmer, 2010), both first instar hatchlings (weighing 1–7 mg) and fifth instar caterpillars (>1 g) are able to cantilever their bodies with only three pairs of attached prolegs for support (Fig. 1A,B). Because complete anesthetization suppresses muscle activation and causes the animals to lose turgor (Fig. 1C), it is apparent that *Manduca* does not possess any structure that has significant bending stiffness. Instead, body stiffness relies on pressurization of the external soft body shell.

To characterize the hydrostatic skeleton in *Manduca* caterpillars, we measured their body length, diameter, volume, density and baseline internal pressure. Caterpillar body pressure is known to be highly variable (Mezoff et al., 2004) because of the internal flow of hemolymph and air cavities (H.T.L. and B.A.T., personal observations) (Wasserthal, 1981). Here, we present a new measurement technique to define the baseline pressure in resting caterpillars. Finally, while previous studies document dramatic morphogenesis of load-bearing tissues, such as the external cuticle, with respect to body mass (Wolfgang and Riddiford, 1981; Wolfgang and Riddiford, 1986), it is unclear how these tissues scale over the entire life cycle of the larvae. We determined the scaling of cuticle thickness and muscle cross-sectional area for *Manduca* caterpillars using histology imaging methods. These data allowed us to numerically evaluate the loading characteristics of the hydrostatic skeleton in the physiological range and during growth.

Hydrostatic skeleton models in biology

The prevailing view of movement by animals without hard skeletons is that they must stiffen their body by pressurizing an internal body cavity such that forces can be transmitted to the substrate instead of being lost to tissue deformation (Chapman, 1958; Trueman, 1975; Vogel, 2003; Wainwright, 1988). For structures consisting of muscles, the muscles can act as both the structural support and the actuator (muscular hydrostats) (Kier, 1992). Although an alternative locomotion strategy based on the controlled release of tension has recently been proposed (Lin and Trimmer, 2010; Simon et al., 2010), it is limited to substrates that are stiffer than the animal. Directed movements on soft media and behaviors involving single point attachments must involve body stiffening, mostly through hydrostatics.

The modeling of biological hydrostatic structures (e.g. cnidarians, annelids and nematodes) generally focuses on morphologies composed of soft tissues without any rigid skeleton (internal or external) supported by pressurized fluid. In particular, it has been shown that soft-bodied animals achieve extreme changes in overall length by using helical reinforcing fibers in the body wall (Clark and Cowey, 1958), a property commonly found in cylindrical biological structures including those of plants (Wainwright, 1982; Wainwright, 1988). To move forward, animals can couple these dramatic extensions with the control of friction or grip (Keller and Falkovitz, 1983). This extension–grip–pull locomotion strategy can be found in many limbless animals, even snakes (Dobrolyubov, 1986).

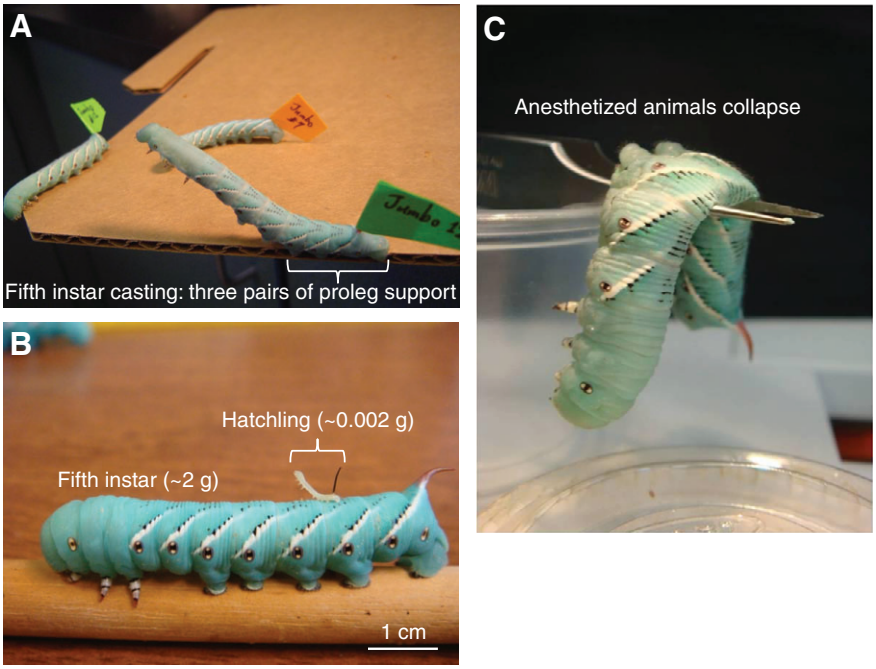

Fig. 1. (A) *Manduca* caterpillars can develop sufficient hydrostatic pressure to cantilever their bodies. (B) During casting behavior, hatchlings three orders of magnitude smaller (by mass) than the fifth instar animals also cantilever their body. (C) Complete anesthetization suppresses muscle tone and causes the caterpillar to lose turgor.

Hydrostatic mechanisms assume, in general, that the fluid content is incompressible and no significant change in body volume occurs, which for most organisms is a reasonable assumption (Chiel et al., 1992; Kier and Smith, 1985; Wadepuhl and Beyn, 1989; Wainwright, 1982; Wainwright, 1988). Finite element models for medical leeches have been created under these conditions (Muller et al., 1981; Sawyer, 1986; Stern-Tomlinson et al., 1986; Wadepuhl and Beyn, 1989). These models incorporate animal geometry, elastic properties of the body wall, internal volume and body pressure to reveal some principles of antagonism in worm-like structures as well as the pressure–volume interactions. As a further step, an empirically based leech model has been implemented with passive tissue properties and muscle activation from motor neurons (Skierczynski et al., 1996). It assumes elliptical cross-sections and constant volume, and simulates the vermiform elongation and pressure changes of a leech. The motions of leeches have also been described using Lagrangian mechanics and a large system of differential–algebraic equations (Alscher and Beyn, 1998) and by modeling a mass transfer wave that describes peristalsis (Accoto et al., 2004; Dobrolyubov and Douchy, 2002).

Although these models describe credible mechanisms for locomotion, they cannot be applied to hydrostatic skeletons that violate the constant body volume constraint. Caterpillars are yet to be described by any of the existing hydrostatic skeleton models for several reasons: (1) extension in the longitudinal direction is accounted for by numerous intersegmental folds instead of body wall stretching (the classical helical fiber-reinforced cylinder model does not apply), (2) body pressure is variable, especially during motion (reflecting fluid flow in the body, not static pressure), (3) the volume may not be constant as the tracheal air can escape (a constant volume assumption cannot be applied), (4) there is no segmental septum that compartmentalizes the animals (localized pressure control is not feasible), and (5) caterpillars are legged systems with discrete on–off attachments (frictional models based on mass transfer do not apply). Additionally, analytical techniques based on linear elastic theory are not applicable, as the mechanical behavior of caterpillar tissues is non-linear and anisotropic. Under typical loading scenarios, these tissues undergo large deformations and have complex boundary conditions. The approach we propose is more general and widely applicable to soft animals because it facilitates structural analyses at different pressure states by relaxing the constant body volume requirement. We treat the hydrostatic skeleton as a shell structure in which the major tissue properties are described by anisotropic, non-linear hyperelastic stress–deformation laws. For any applied body load, the body deformation is determined using large deformation theory and the material models developed in previous studies. This approach provides a more realistic approximation of a caterpillar's hydrostatic skeleton. For simplicity in this study, we evaluated only the static conditions.

MATERIALS AND METHODS

Experimental animals

Manduca sexta L. larvae were reared on an artificial diet in an incubator at 27°C with a light:dark cycle of 17:7 h (Bell and Joachim, 1976). Third to fifth instars were selected for experimentation, ranging from 0.01 to 3 g in mass. Twenty animals were used for biometry measurements, 39 animals for histology imaging, 27 for the body density measurement, 14 for determining the net tissue density and 32 for the baseline pressure measurements.

Load-bearing tissue quantification

Tissue fixation and histology

Animals were killed by exposing them to ethyl acetate fumes for 30 min. They were then fixed using 10% formalin with phosphate-buffered saline (PBS) and 10% dimethyl sulfoxide (DMSO) for 24–48 h until the external cuticle became rigid enough for slicing. The thoracic segments and terminal segments were removed from all animals to facilitate fixative perfusion. If possible, the gut content was also removed with the peritrophic membrane, leaving the interior hollow and allowing better penetration of the fixative. The third abdominal segment (A3) was sectioned from each animal with all muscle attachments intact. The samples were then kept in the same formalin mixture and sent to Tufts Cummings School of Veterinary Medicine Histology Lab for paraffin embedding and slicing. Cross-sectional slices (10 µm) were taken from the middle of segment A3 in all samples and stained with hematoxylin and eosin (H&E). Typically H&E stains cell nuclei blue and many proteins in the cytoplasm pink. The result allowed us to distinguish muscles from the cuticle and epithelium layers on the histology slides. Selected samples of the fifth abdominal (A5) segment were

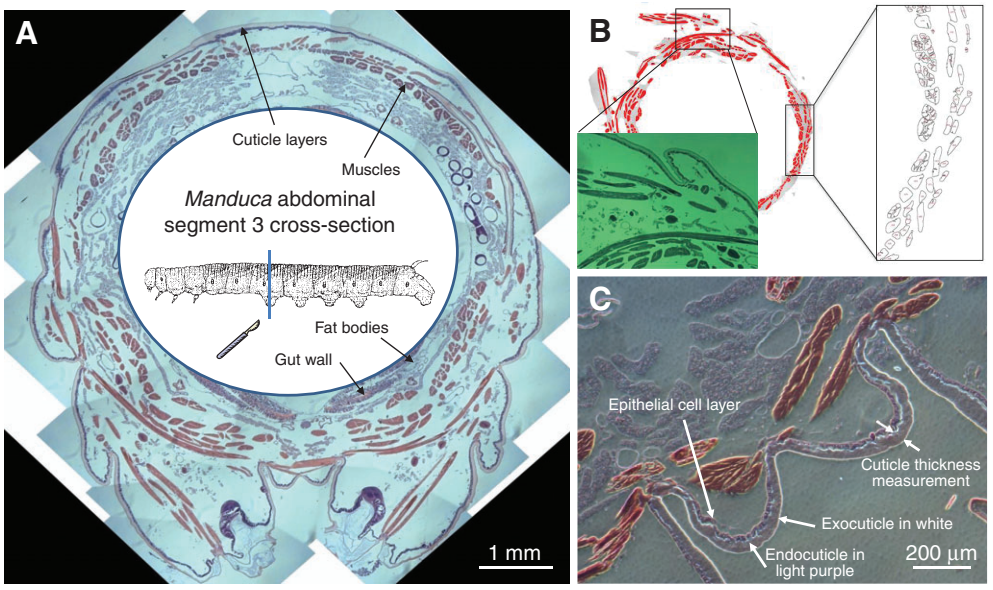

Fig. 2. Histology of *M. sexta* caterpillar. (A) Adjacent histology images of abdominal segment 3 were obtained by merging multiple microscopic images. The example cross-section came from a fifth instar animal. Hematoxylin and eosin (H&E) stained most of the soft tissues inside the body. (B) Blue light excitation (observed in green) emphasized muscle fibers so that they could be identified by image analysis. (C) The endocuticle and exocuticle layers are easily distinguished from the soft flaky epithelial cell layer, which was excluded from the cuticle thickness measurements. The gut wall is orders of magnitude softer than the muscle fibers in the longitudinal direction and cuticle in the circumferential direction. It was therefore omitted in measurements of mechanical components.

prepared in the same way, but we found no evident difference from the tissue thickness of A3 samples. All scaling measurements were therefore obtained from A3 samples.

Imaging and image analysis

The histology cross-sections were imaged with a Zeiss Axiovert 40 CFL inverted microscope with standard dichromic mirrors (Fig. 2). Image collection was performed using QCapture Pro (QImaging, Surrey, BC, Canada). Color was autobalanced prior to collecting images and all images were collected at ×5 magnification with a 2560×1920 acquisition resolution. It was found that the blue excitation light produced the most contrast between the muscles and the surrounding tissues. Because the sections were too large to view as a single image, multiple images were taken and merged using the Photomerge function in Adobe Photoshop (Adobe Systems, Inc., San Jose, CA, USA). For the larger images, the resolution was halved during the image merging process. All image analysis was done using ImageJ (NIH). First, a global calibration scale was applied by imaging a hemocytometer with lines of known length. Next, the cuticle thickness was measured along the ventral body wall between the prolegs (a location that can be easily identified in all slides). A mean thickness was obtained from five measurements. All cuticle thickness measurements were taken from A3 sections. Next, all easily discriminated non-muscle structures were manually removed from the image. The image was then converted to an 8-bit grayscale image and a grayscale histogram analysis was performed. Typically, two peaks were observed on the histogram, one representing the muscles and the other representing other structures and background noise. A threshold was set between these two peaks and the image was then converted to a binary image containing only muscle. Using the 'analyze particles' function, the area of each muscle was determined and summed to yield the total cross-sectional muscle area. Before accepting the particle analysis, each image was checked manually and cross-referenced with the original image to ensure that the particles being counted represented all muscles and were specific to only muscles.

Body density measurements

The overall body density of third, fourth and fifth instar *M. sexta* larva was determined by comparing the animal's body weight in the air and under water. First, an isometric force transducer (Grass Products Group, West Warwick, RI, USA) was calibrated with objects of known mass. The caterpillars were then placed on a substrate (made of 2.4 mm diameter carbon fiber rod encapsulated by silicon tubing and sealant) suspended from the force transducer. The air weight of the caterpillar was measured by subtracting the transducer offset due to the substrate. The measured air weight was repeatable within 1% of the animal mass, determined from a Mettler laboratory scale (0.1 mg accuracy). The animal was slowly lowered into a beaker of de-ionized water at room temperature containing a few drops of surfactant to reduce surface effects upon submersion. The buoyant force of the caterpillar was calculated from the submerged total weight by subtracting the pre-determined effect of substrate immersion alone. Dividing the animal's body weight by its measured body volume gave the overall body density. Changes in water density due to surfactant and temperature were insignificant compared with the accuracy of the force transducer.

Tissue density measurements

Tissue density was determined by homogenizing third, fourth and fifth instar *M. sexta* in 0.2 ml (for animals less than 0.5 g) or 0.5 ml (for larger animals) *Manduca* saline (6.5 mmol l^{-1} NaCl, 33.5 mmol l^{-1} KCl, 16.2 mmol l^{-1} $MgCl_2$, 13.6 mmol l^{-1} $CaCl_2$, 166.5 mmol l^{-1} dextrose, 1.25 mmol l^{-1} $KHCO_3$ and 1.25 mmol l^{-1} KH_2PO_4) (Weeks and Truman, 1984). This dilution resulted in a 1:2 to 4:1 animal to saline ratio, with the smallest total volume of at least 0.3 ml. The remaining tissue fragments were further broken down using a sonifier (Branson Ultrasonics Inc., Danbury, CT, USA) for 15 s at 20% power. This mincing and sonication process was repeated until a smooth tissue homogenate was produced. The samples were then centrifuged for 2 min to remove any remnant air vesicles in the tissue solution, which allowed the final sonication step to produce a solution of uniform density. A fixed volume (0.1 ml for animals less than 0.5 g and 0.2 ml for larger animals) of the homogenate was extracted with a calibrated pipette and weighed to calculate the density. The measured density was then scaled up to account for the previous saline dilution. This sampling was performed twice per animal to obtain the mean tissue density.

Body pressure measurements

In preliminary measurements of *Manduca* body pressure fluctuation, silicon catheters (i.d. ~0.8 mm, o.d. ~1 mm) were inserted into the tail horn of mildly anesthetized caterpillars and connected to a small silicon piezoresistive pressure sensor (Honeywell, Freeport, IL, USA). These recordings revealed small, rhythmic pressure fluctuations (data not shown) that matched the *Manduca* caterpillar heart rate (Smits, 2000) and were attributed to hemolymph flow produced by the dorsal vessel and abdominal contractions (Sláma, 1984; Sláma, 2003). As the animals resumed motion, the pressure changed inconsistently, rising or falling with the smallest movements and making this method inappropriate for establishing the static pressure range of a resting caterpillar.

An alternative method was therefore used based on balancing fluid height in a capillary pipette. To minimize movements, the animals were uniformly air chilled to 10–15°C using a cold chamber. This temperature does not anesthetize the animals and is the minimum at which the muscles still respond to stimulation in the normal way (W. Woods, personal communication). Thin acupuncture needles (0.12 mm diameter; Seirin-America, Weymouth, MA, USA) were used to introduce a weak point on the dorsal posterior cuticle surface to one side of the dorsal midline. A glass micropipette (tip i.d. ~0.1 mm, tip o.d. ~0.15 mm, tube o.d. 1 mm) was then wedged into the body at this weak point and hemolymph was drawn into the tube by capillary action aided by the internal body pressure. An adjustable water column was connected to the other end of the capillary tube to counterbalance the hemolymph pressure by forcing the hemolymph back into the animal. This water column also buffered transient pressure fluctuations and its height was recorded and converted to units of pressure. This method was calibrated using a silicone rubber 'caterpillar mockup' with controllable internal pressure (a large water column reservoir, Fig. 3A). During calibration the height of the water column directly mapped to the height of the water reservoir with a constant offset determined by the capillary effect of each glass pipette. A pressure transducer was used to detect any pressure fluctuation during each measurement. Typically, it took 5 s to reach equilibrium and readings were repeatable within 8% (54 calibration samples). Most animals were not responsive during glass pipette insertion (Fig. 3B) and some survived to pupation.

Biometry measurement

Caterpillar bodies are fairly cylindrical (Fig. 2A). To determine scaling of the hydrostatic skeleton, we measured the body length

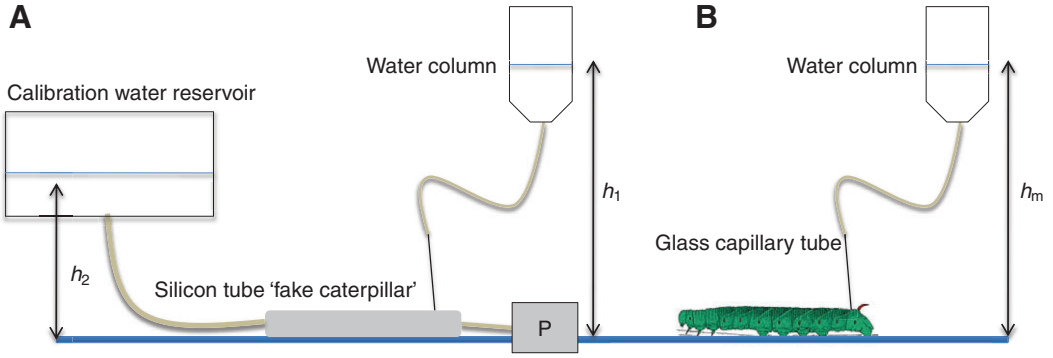

Fig. 3. Baseline body pressure measurement. (A) To calibrate pressure measurements using the capillary system, a 'fake caterpillar' was constructed from silicon tubing similar in diameter to the animal. The internal pressure was controlled and buffered by a large water reservoir. The linearity of the change of pressure was independently monitored by the pressure transducer, P, on the other end. A glass capillary micropipette was inserted into the fake caterpillar to assess the internal pressure. The level of the water column h_1 was mapped to the calibration water reservoir h_2 in the calibration process. (B) The pipette was then inserted into a live *Manduca* to obtain a baseline resting pressure using the height of the water column h_m.

and radius of caterpillars over a wide size range (Fig. 4). The body radius was defined as one half of the mean height of the first, third and seventh abdominal segments viewed in the sagittal plane. Measurements were made from resting caterpillars photographed on a calibrated substrate using ImageJ.

Scaling data analysis

By convention, biological scaling data are modeled as a power function using the slope of a linear regression of each measured parameter plotted against body mass on a logarithmic plot. The slope obtained in this way represents the power by which the measured parameter scales with body mass. We use the terms 'scaling factor' and 'scaling power' interchangeably throughout this paper when referring to this important scaling constant. For any object that scales isometrically, the linear dimension would scale as a power of 1/3 and area 2/3 with respect to the volume. Assuming a constant density (very small variation in caterpillars), the isometric scaling power would be 0.33 for a linear dimension and 0.67 for an area. To evaluate the ontogenetic scaling of various biometrics in caterpillars, we compared the scaling factors from the experimental data against a reference value using Student's *t*-statistics (Quillin, 1998). All the isometric reference curves in this study were constructed by scaling up the lowest values in the experimental data with the isometric scaling factors.

RESULTS

Manduca body aspect ratio

Biometric data from our *Manduca* colony show that the overall body length and radius scale allometrically but are not far off isometric predictions (Fig. 4). Caterpillars generally grow from a slender body aspect ratio to a stouter one. Based on our data, the diameter:length aspect ratio scales from 0.118 to 0.137 (from a hatchling to a ~2 g fifth instar). Other species of caterpillar have much more dramatic allometric body scaling (H.T.L. and B.A.T., personal observation).

Manduca cuticle ontogeny and muscle development

Both the mean thickness of the endocuticle layers and overall muscle cross-sectional area scale allometrically, even though the data are very close to the isometric predictions (Fig. 5). The cuticle thickness scaling power was 0.43, which is significantly larger than the 0.33 isometric power (t=2.52, P=0.008, d.f.=37). The muscle cross-sectional area increased in a step-wise manner at the beginning of each instar but roughly along the isometric reference (0.67). The typical ecdysis mass values were derived from an empirical *Manduca* growth model (Nijhout et al., 2006). Because of the technical difficulty of fixing all the internal structures, only 13 animal samples (out of 39 animals) allowed total muscle cross-section measurements on the A3 segment.

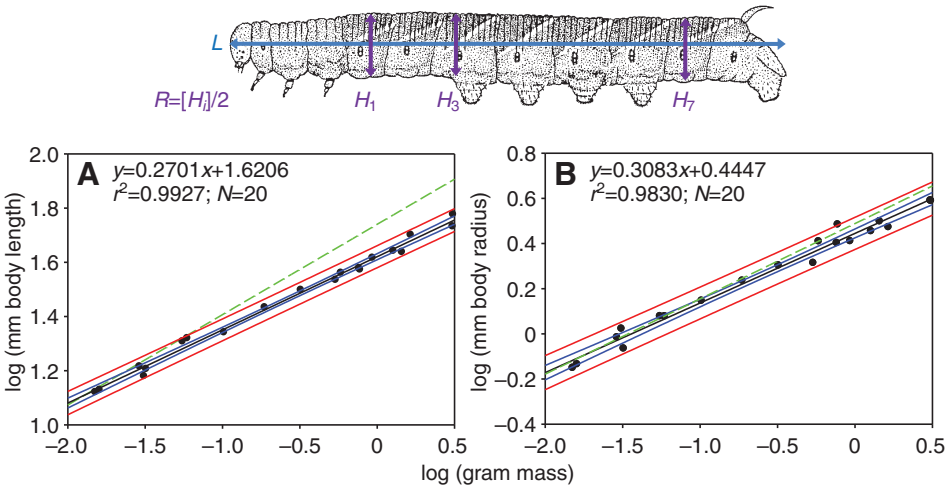

Fig. 4. Ontogenetic scaling of *Manduca* body proportions. Body length (L) was measured between the head capsule and anus, while body radius (R) was defined to be one half of the mean height measured at segments 1 (H_1), 3 (H_3) and 7 (H_7) in the calibrated images. Both quantities increased as a power function of body mass (A,B). Both linear regressions significantly deviate from the isometric slope of 0.33 (green dashed line) as demonstrated by the two-tail t-tests for body length (P<0.001) and radius (P=0.0346). The 95% confidence band and 95% predicted band are plotted in red and blue, respectively.

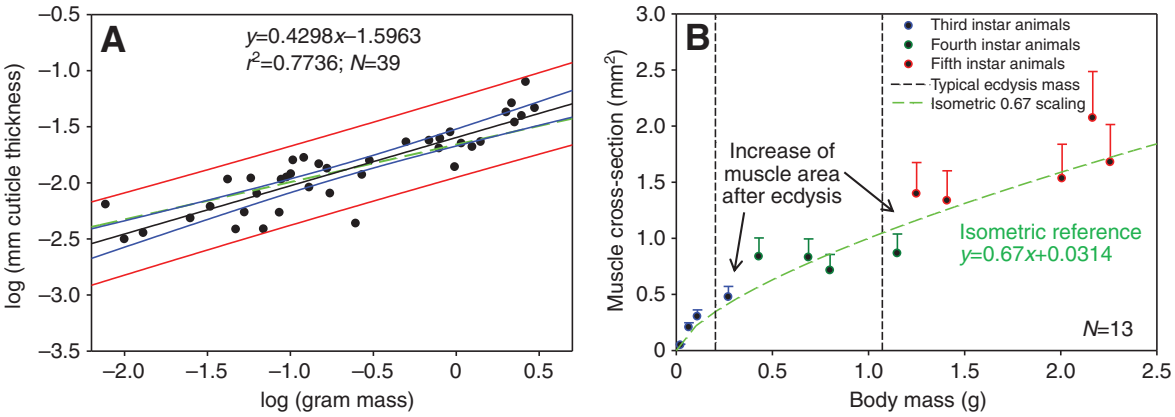

Fig. 5. Ontogenetic scaling of *Manduca* cuticle and muscle. Load-bearing tissues thicken in developing *Manduca* caterpillar as measured by histology imaging. (A) Cuticle thickness increases with a power of 0.4298 with respect to body mass, which is significantly greater than the isometric scaling of 0.33 for a linear dimension (P<0.05, test power 0.8153). However, given the variation, the isometric reference line (green dashed curve) is still well contained in the 95% predicted interval (red lines). The 95% confidence band is plotted in blue. (B) Muscle cross-sectional area increases stepwise at ecdysis so curve fitting cannot be applied (therefore not shown in logarithmic scales). However, the data closely follow the isometric scaling power (0.67, green isometric reference curve).

Manduca body volume scaling

Manduca caterpillars become water buoyant after they molt into fifth instar. By comparing the air weight and submerged water weight of the same animal, the body volume can be estimated for a range of animals from third to fifth instar. The scaling coefficient of volume and mass on a logarithmic plot is 1.0184±0.0046 (r^2=0.9997) with an almost negligible y-intercept. This suggests that *Manduca* caterpillars become less dense than water when they exceed 1 g of body mass, crossing the point (0,0) on a log plot (Fig. 6A). This corresponds to the expected body mass (1.071 g) at the end of the fourth instar (Nijhout et al., 2006). A one-sample, two-tailed Student's t-test revealed that the 1.84% extra volume expansion is significantly different from the constant density unity scaling coefficient (t=4.03285, P<0.001, d.f.=25). *Manduca* caterpillars decrease in density as they get larger. While the accumulation of body fat could account for this change in body density (Tsuchida and Wells, 1988), it could also result from changes in the tracheal system. Our data show decreasing trends with non-zero slopes in both the mean body density (t=–4.0178, P=0.0005, d.f.=25) and the net tissue density (t=–3.0925, P=0.0093, d.f.=12) (Fig. 6B). However, these two parameters also decrease with the same exponential power (slopes) (t=1.2132, P=0.2327, d.f.=37), suggesting that changes in body density are predominantly due to increasing body fat or other low-density tissue growth. Nevertheless, the air cavity volume (as a percentage of the total body volume) increases significantly from 2.87% for a 0.05 g animal to 7.69% for a 2 g animal. This large volume of internal gas could influence dynamic loading of the hydrostatic skeleton.

Manduca baseline body pressure

Even under carefully controlled conditions, *Manduca* baseline pressure varied widely, with most measurements clustering between 1 and 1.6 kPa (Fig. 7). Although body pressure tended to be lower in larger animals, there was no satisfactory linear regression to this trend (r^2<0.2). Evidently, caterpillars in different stages can function in a similar pressure range. The mechanical consequences of this large operation pressure range were evaluated using a non-linear finite element model, as discussed below.

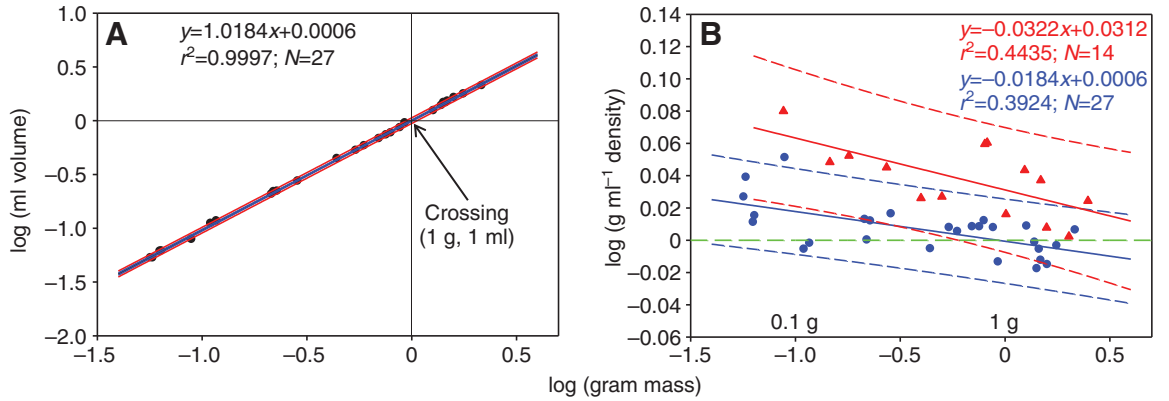

Fig. 6. Ontogenetic scaling of *Manduca* overall body density and net tissue density. (A) Plotted on a logarithmic scale, a regression line of body volume as a function of body mass passes through the null intersect (0,0), indicating that animals heavier than 1 g were less dense than water. The slope is significantly different from unity (P<0.001). (B) Body density (in blue) and tissue density (in red) both decline in developing caterpillars and the slopes are both significantly different from zero (body density P<0.01, tissue density P<0.001) but not significantly different from each other (P=0.1158). The red and blue dashed lines represent the 95% predicted bands, which overlap greatly. Despite the large variation, the decrease of overall body density is quite evident.

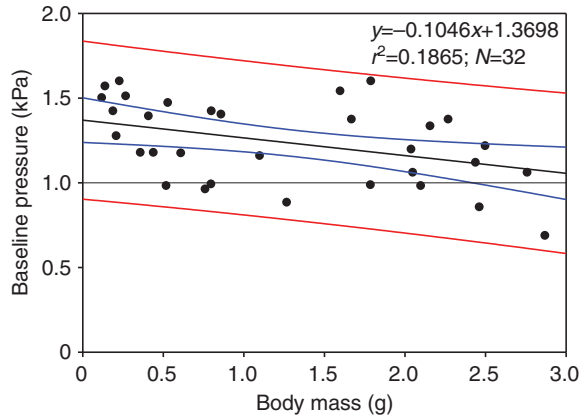

Fig. 7. *Manduca* baseline body pressure. Resting body pressure was between 1 and 1.6 kPa in most animals, but in larger animals it could drop below 1 kPa on occasions. There was no valid scaling power, and the linear regression shows poor correlation despite the apparent trend. Most animals operate with a resting body pressure higher than 1 kPa.

Modeling a hydrostatic skeleton

Unlike engineered structures, it is difficult to subject living animals to standard mechanical tests. As an alternative approach, mathematical and numerical models can be used to investigate and predict the structural responses of animals. There has been a great deal of effort in developing analytical solutions for inflatable structures, going beyond elementary beam bending theory (Le Van and Wielgosz, 2005; Thomas et al., 2006). To remove constraints and simplifications associated with analytical solutions, we developed an empirically based numerical approach to explore the mechanical responses of the hydrostatic skeleton in caterpillars. The ontogenetic scaling data presented in this paper provide realistic values with which to implement a numerical simulation.

Caterpillar hydrostatic skeleton

Caterpillars have a very complex, multi-scale structure with body weight and other applied loads jointly supported by the cuticle and muscles. Experimental results show that the mechanical response of the cuticle in the longitudinal and circumferential directions is highly non-linear, with stresses increasing exponentially with stretch (Lin et al., 2009). For a given stretch, stresses are larger for cuticle specimens loaded in the circumferential direction than for specimens loaded in the longitudinal direction, indicating anisotropy in the material response (Fig. 8A). In particular, greater stiffness in the circumferential direction is necessary to support hoop stress generated by pressurization. Muscles are primarily oriented in the longitudinal direction and can be activated to increase body pressure. A detailed description of the mechanical response of the ventral interior lateral muscle of A3, both with and without stimulation, is given in recent publications (Dorfmann et al., 2007; Dorfmann et al., 2008; Lin et al., 2009).

Our data show that muscles have deformation-dependent properties, exhibit loading–unloading hysteresis and are capable of increasing stiffness during stimulation. The effect of the stimulus depends non-linearly on the amount of deformation (Fig. 8B). All other tissues of *Manduca* are highly compliant relative to the cuticle or muscles. While these tissues do not carry a significant load, they are necessary to maintain internal pressure and to prevent the cuticle from collapsing. Also, leg structures are protrusions that do not affect the overall stiffness of the hydrostatic skeleton.

Finite element model

To model the hydrostatic skeleton of a caterpillar, we considered an inflatable, horizontal, cylindrical tube with a circular cross-sectional area. The shell of this tube was composed of two groups of perfectly aligned, homogeneous, superimposed fibers. Fibers in the circumferential direction accounted for the anisotropic behavior of the cuticle (Fig. 8A); fibers in the longitudinal direction accounted for the behavior of major body muscles. The muscles could be switched between passive (tonic) and active (tetanus) states (Fig. 8B). In the proposed model the total length is denoted by L, the radius by R, the cuticle layer thickness by t_1 and the equivalent muscle layer thickness by t_2 (Fig. 9). We assumed that the total cross-sectional muscle area could be spread uniformly around the perimeter of the model. Therefore, the muscle layer thickness t_2 is given by the equality $2\pi Rt_2$=total cross-sectional muscle area. Two shell layers having thicknesses t_1 and t_2 are superimposed and share the same nodal points, in accordance with the parallel modeling approach (Nelson and Dorfmann, 1995). Finally, the left end of the finite element model is restrained to eliminate any rigid body motion, while the right end is capped.

The constitutive equations used to describe the non-linear mechanical response of the cuticle in the longitudinal and circumferential directions are based on an exponential stress-stiffening formulation (Fig. 8A) (Lin et al., 2009). The force–extension characteristics of *Manduca* muscles under constant-rate loading and unloading can be simulated using a pseudo-elastic reinforcing model both in a passive state and during tetanic stimulation (Fig. 8B) (Dorfmann et al., 2007). In addition to strain-dependent stress softening, the responses of *Manduca* muscle depend on the rate of loading and unloading (Dorfmann et al., 2008). For the purposes of this work, we focused on the time-independent formulation, thereby ignoring rate and viscous effects. To examine the effects of scaling on caterpillar hydrostatic skeletons, we considered the sizes of a fifth instar and a hatchling *Manduca*. Table 1 summarizes the values of the geometric parameters used for both size scales. In addition, we

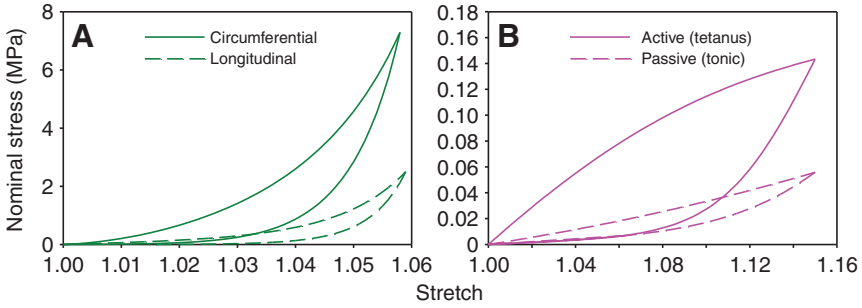

Fig. 8. Material properties of caterpillar cuticle and muscles. (A) The soft cuticle of *M. sexta* has a variable stiffness that increases with increased stress. The solid curve represents the cuticle loaded in the circumferential direction while the dashed curve shows the loading behavior in the longitudinal direction. Note that the cuticle is stiffer in the circumferential direction, presumably accounting for the lack of circumferential muscles. (B) *Manduca* muscles also exhibit pseudo-elastic behavior in both the active (tetanus) state (solid curve) and passive (tonic) state (dashed curve). These highly non-linear behaviors cannot be approximated by any analytical models based on linear elastic theories.

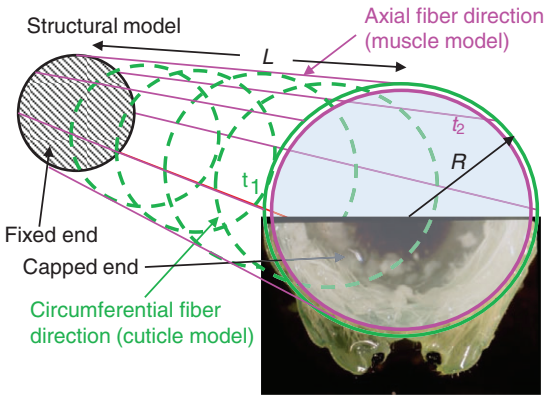

Fig. 9. Structural model of the hydrostatic skeleton in caterpillars. The hydrostatic skeleton in the caterpillar was realized as an inflatable cylindrical tube with transverse isotropy due to fiber reinforcement. The body length L, radius R, body wall thickness t_1 and equivalent muscle layer thickness t_2 were derived from the animal biometric data fits at body masses of 2 and 0.05 g, respectively (see Table 1). The body wall contains two sets of fiber reinforcement, the first in the circumferential direction characterized by cuticle mechanics (cuticle thickness) and the second characterized by muscle mechanics. The muscle's stress-dependent stiffness simulates the behavior of *Manduca* muscles in either the tetanus or the tonic condition.

considered muscle fibers to be in either an active (tetanus) or passive (tonic) state. With the two possible size scales and the two muscle conditions, we considered four models in total.

Each of the four models was analyzed following a two-step process. During the initial step, pressure was applied to the inner surface of the cylindrical tube and to the cap at the free end. This pressure increased monotonically to a predefined target value. During pressurization, the model was subjected to longitudinal extension and radial inflation. The correlation between the change in radius R and the change in length L, at a given pressure, was non-linear and depended on the magnitude of the geometric parameters, the cuticle stiffness, the passive properties of the muscles and the force developed during activation. The resulting stable deformed configuration was cylindrical with a circular cross-section and the longitudinal axis pointed in the horizontal direction. In the second step of the analysis, a body force was added with the vertical component gradually increasing from zero, with the applied pressure held constant. We monitored the vertical deflection of the free end until the configuration became unstable following a compression buckling mode, localized at the fixed end. The model detailed here was implemented in the non-linear finite element package Abaqus (Simulia, Providence, RI, USA). The above two-step procedure decoupled the body pressurization from muscle activation, and therefore allowed us to simulate the hydrostatic skeleton at any target state.

Table 1. Modeling parameters derived from the experimental scaling data fits for two body sizes

	Small body size (0.05 g)	Large body size (2 g)	Scaling factor
L	18.6 mm	50.3 mm	0.27
R	1.10 mm	3.45 mm	0.31
t_1	0.007 mm	0.034 mm	0.43
A	0.144 mm^2	1.71 mm^2	~0.67
t_2	0.021 mm	0.079 mm	Derived from A

L, body length; R, body radius; t_1, body wall thickness; t_2, muscle layer thickness; A, area.

The results of the four models are reported as normalized body force *versus* normalized tip deflection. The body force was normalized by the selected body masses (2 g and 0.05 g) and the tip deflection by the initial body length L. The geometric dimensions of the undeformed configuration were derived from the experimental fits presented above. The total cross-sectional area of the muscles was assumed to be isometric (0.67 power scaling) (Table 1). The initial slope of the normalized body force as a function of the normalized tip deflection was used to define the specific bending stiffness (a dimensionless parameter in this case).

Modeling results

At any given internal pressure, the model tip deflection increased linearly in the initial phase with applied body force up to a critical point (examples are given in Fig. 10). The specific bending stiffness of the large scale model was much lower than that of the small scale model. This is the combined result of the increasing bending moment and the scaling of overall structural parameters (Table 1). In addition, previous studies on inflatable beams (with a linear-elastic membrane) showed that pressurization delayed the buckling deflection but had little effect on the initial flexural stiffness (Fichter, 1966; NASA, 1965; Veldman et al., 2005). In contrast, the results from our finite element simulation show how an increasing pressure directly stiffens the structure (increase in initial slope). This is due to the non-linear, stress-stiffening properties in the tissues and the large deformation kinematics considered in the analysis.

The bending stiffness increased non-linearly with increasing internal pressure (Fig. 11) across the two model sizes, and the two muscle states, passive (tonic) and active (tetanus). The resulting trends clearly show that the increase in stiffness due to pressurization is much higher for the smaller model (by at least an order of magnitude as shown in the semi-log plot in Fig. 11). Also, the increase in stiffness is more pronounced at low values of internal pressure, becoming less significant at high pressures.

The effect of cuticle thickness on model stiffness was very revealing. Specifically, we considered the small scale model with muscle in the passive (tonic) state and with an internal pressure of 1 kPa (typical body pressure in *Manduca*). We doubled the cuticle thickness t_1 from the original value of 0.007 mm to 0.014 mm. Contrary to intuition, the model appeared softer during loading, and became unstable at a smaller applied body force. This is a direct consequence of the non-linear constitutive model used for the cuticle. The exponential increase in stress with applied stretch is equivalent to an increase in stiffness with increasing load in the cuticle (Fig. 8). For a given internal pressure, the increase in cuticle thickness reduces the hoop and longitudinal stresses and therefore the material stiffness. A similar argument applies, but to a lesser extent, when the total cross-sectional area of the muscles is increased (Fig. 11).

DISCUSSION

Our findings have several implications for the use of a hydrostatic skeleton for body support. First of all, bending stiffness in a pressurized cylinder with a hyperelastic shell is determined by three major factors: internal pressure, shell wall thickness and material properties. Baseline internal pressure dictates the amount of stress in the shell wall before a body load is applied. Shell wall thickness determines the distribution of this stress. The non-linear material properties relate the stress in the shell wall to the resulting strain which produces the structural deformation. These three parameters therefore have a major impact on the initial conditions and structural stiffness of an inflated cylinder. Of course, whether this stiffness is sufficient to allow the body to be functional when cantilevered

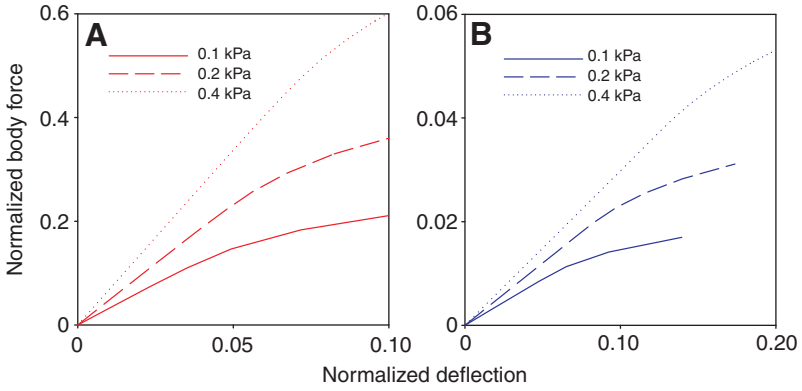

Fig. 10. Sample results for the finite element model of the hydrostatic skeleton in caterpillars. (A) Flexural tests can be performed on the finite element model at any constant pressure. Example curves from 0.1, 0.2 and 0.4 kPa pressure are shown for the small model (body mass 0.05 g). Body force was evenly distributed to all the finite elements and normalized to the body mass derived from the model sizes listed in Table 1. Model tip deflection was normalized to the initial model body length *L*, as also given in Table 1. (B) The corresponding curves from the large model (body mass 2 g) are shown. It is evident that the small model has a much greater bending stiffness given the same internal pressure.

depends on the body loading condition, which comes from the overall body dimensions and body weight.

There are two major mechanisms to control the body stiffness in caterpillars; body pressurization and muscle activation. Body pressurization stretches the body shell in the longitudinal and circumferential directions. Because of the stress-stiffening property of the tissues, the overall body bending stiffness increases in response to pressurization. However, the stiffness eventually plateaus as the stress-stiffening effect diminishes in the tissues at high stress states. Further stiffening can be achieved by muscle activation, which not only increases body shell stiffness but also resists body elongation. The animals are most likely to employ the two mechanisms simultaneously. This study explored these two mechanisms independently in order to reveal the range of capable states a caterpillar can achieve. The next step will be to examine how muscle activation determines body volume and pressure.

Curiously, increasing muscle cross-sectional area or cuticle thickness will not result in higher structural bending stiffness for a given internal pressure. For a pressurized cylindrical shell, an increase in the wall thickness decreases the stress for the same applied forces (i.e. internal pressure). To stress the added material to the same state, the hydrostatic skeleton has to operate at a higher baseline pressure, which may not be ideal for the animal. This may be why caterpillars such as *Manduca* maintain almost isometric scaling for muscle and cuticle thickness.

Alternatively, the animal can solve the body support problem by simply limiting its size. As the body load scales with body volume, and the body dimensions scale almost linearly, overall size reduction alleviates the body load dramatically. For an inflatable cylinder with a constant internal pressure, the hoop stress is proportional to the body radius and disproportional to the body wall thickness. In *Manudca* caterpillars, slight allometric scaling in the body wall implies higher hoop stress in small hydrostatic skeletons. This puts stress-stiffening material under a higher initial stress. Consequently, small hydrostatic skeletons are actually operating at higher stress for the same pressure. Of course, changing the body diameter:length aspect ratio could affect the overall structural stiffness and the loading condition. Therefore, another simple solution to improve body support is to change the aspect ratio with increasing body size, as seen in most caterpillars. This is in fact quite dramatic in some caterpillar species where the hatchling has a diameter:length ratio of ~0.1, which triples to ~0.3 in the last instar (H.T.L. and B.A.T., unpublished data). In fact, some small inchworms can also maneuver and remain stable even with a diameter:length ratio of ~0.05.

The above analyses may allow us to address an important dichotomy in caterpillar locomotion: why do some inch and others crawl? Inching involves well-controlled casting behavior to find a target substrate and precise placement of the posterior legs to meet the anterior ones. This mode of locomotion requires an effective hydrostatic skeleton and body coordination as predicted in computer simulations (Ghanbari et al., 2008). On the other hand, crawling can be identified by the propagation of an anteriograde body contraction wave (Snodgrass, 1993). This mode of locomotion does not necessarily rely on a hydrostatic skeleton. Ground reaction force analysis of *Manduca* locomotion shows that a crawling caterpillar can use the substrate as an 'environmental skeleton' to transmit compressive forces while keeping most of the body in tension (Lin and Trimmer, 2010). Why do different species of caterpillar adapt inching and/or crawling while sharing the same general body anatomy? The answer could simply be a matter of size. There might be a mechanical limitation to maneuvering primarily with a hydrostatic skeleton when the caterpillar is big.

Hydrostatic body support for large caterpillars requires muscle activation and significant pressurization. To avoid constant high pressure in the body and to minimize muscle work, large caterpillars

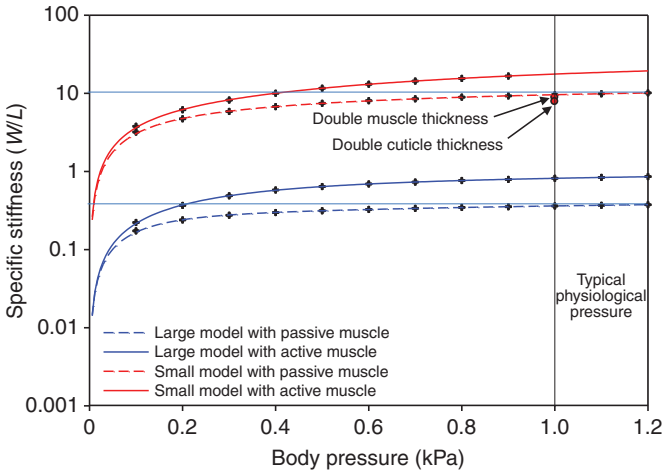

Fig. 11. Normalized body stiffness comparison. The hydrostatic skeleton model was tested at two sizes and for two muscle states (data plotted on semi-log scale). A simple spline fit was applied to illustrate the trends. The active state simulates when the muscles were receiving tetanic stimulation, while the passive state represents resting muscles with proper muscle tone. The overall structural stiffness (applied load in body weight *W*/tip deflection in body length *L*) was much greater in small models (red) than in large models (blue) by more than one order of magnitude. Interestingly, as the models enter the typical physiological pressure range, the stiffness plateaus in all cases. Muscle activation roughly doubles the structural stiffness in this range.

keep their body aligned with the substrate most of the time, supported by closely spaced prolegs. Small caterpillars, on the other hand, can easily achieve self-supporting body stiffness even with muscle in the tonic state. The hydrostatic skeleton can operate at normal physiological pressure and the body responds to muscle control dynamically. Under these conditions, smaller caterpillars do not need many leg supports and inching becomes an appealing locomotion strategy, especially when they are very small compared with the branched plant structures. This argument may apply to all small caterpillars, as well as hatchlings of large caterpillars. Why then does *Manduca* not change from inching to crawling as it grows? Perhaps such a switch is difficult for the control of prolegs as it involves a major modification of the gripping pattern. It is interesting to note, however, that *Manduca* caterpillars in the first two instars have noticeably smaller mid-abdominal prolegs (more like inchworms). It is very likely that hatchlings spend more time picking up their bodies in search of new food substrates. In fact, gait switching has been reported in some caterpillar species during development (Hinton, 1955). An extensive behavioral survey should be able to confirm this hypothesis.

CONCLUSIONS

To summarize, we have determined the biometric scaling of *Manduca* caterpillars over two orders of magnitude of body mass during development. The body density and baseline pressure drop only slightly. Combining these new scaling data with two previously published constitutive models of caterpillar muscles and cuticle, we used a non-linear finite element model of an inflatable cylinder to represent the hydrostatic skeleton of a caterpillar. This model shows that increasing body pressure has a direct impact on the overall bending stiffness up to the physiological pressure range. Starting from the minimum physiological pressure, any increase of body pressure does not give rise to a significant increase in structural bending stiffness. However, muscle activation can double this stiffness regardless of body size. The model also demonstrates that near-isometric scaling can decrease the overall bending stiffness dramatically. Although the initial parameters were based on *Manduca*, this modeling approach can be applied to different body forms and sizes. It can be used to examine mechanical constraints on caterpillars of different sizes or species. More specifically, the decrease of inherent stiffness due to up-scaling may impose a great biomechanical cost to large caterpillars and therefore lead to a behavior preference for crawling. In contrast, inching is much more commonly found in caterpillars with small bodies.

ACKNOWLEDGEMENTS

We would like to thank Ethan Golden for his connection to the Tufts Veterinary School and his assistance in the caterpillar histology fixation. This research is funded by NSF grant IOS 0718537 to B.A.T. and NSF grant IOS 0909953 to H.T.L.

REFERENCES

Accoto, D., Castrataro, P. and Dario, P. (2004). Biomechanical analysis of Oligochaeta crawling. *J. Theor. Biol.* **230**, 49-55.
Alscher, C. and Beyn, W. J. (1998). Simulating the motion of the leech: a biomechanical application of DAEs. *Numerical Algorithms* **19**, 1-12.
Bell, R. A. and Joachim, F. G. (1976). Techniques for rearing laboratory colonies of tobacco hornworms and pink bollworms. *Ann. Entomol. Soc. Am.* **69**, 365-373.
Bura, V. L., Rohwer, V. G., Martin, P. R. and Yack, J. E. (2011). Whistling in caterpillars (*Amorpha juglandis*, Bombycoidea): sound-producing mechanism and function. *J. Exp. Biol.* **1**, 30-37.
Chapman, G. (1958). The hydrostatic skeleton in the invertebrates. *Biol. Rev.* **33**, 338-371.
Che, J. and Dorgan, K. M. (2010). It's tough to be small: dependence of burrowing kinematics on body size. *J. Exp. Biol.* **213**, 1241-1250.
Chiel, H. J., Crago, P., Mansour, J. M. and Hathi, K. (1992). Biomechanics of a muscular hydrostat: a model of lapping by a reptilian tongue. *Biol. Cybern.* **67**, 403-415.
Clark, R. B. and Cowey, J. B. (1958). Factors controlling the change of shape of certain nemertean and turbellarian worms. *J. Exp. Biol.* **35**, 731-748.
Demetrius, L. (2006). The origin of allometric scaling laws in biology. *J. Theor. Biol.* **243**, 455-467.
Dobrolyubov, A. I. (1986). The mechanism of locomotion of some terrestrial animals by travelling waves of deformation. *J. Theor. Biol.* **119**, 457-466.
Dobrolyubov, A. I. and Douchy, G. (2002). Peristaltic transport as the travelling deformation waves. *J. Theor. Biol.* **219**, 55-61.
Dorfmann, A., Trimmer, B. A. and Woods, W. A. (2007). A constitutive model for muscle properties in a soft-bodied arthropod. *J. R. Soc. Interface* **4**, 257-269.
Dorfmann, A. L., Woods, W. A. and Trimmer, B. A. (2008). Muscle performance in a soft-bodied terrestrial crawler: constitutive modeling of strain-rate dependency. *J. R. Soc. Interface* **5**, 349-362.
Fernando-Warnakulasuriya, G. J. P., Tsuchida, K. and Wells, M. A. (1988). Effect of dietary lipid content on lipid transport and storage during larval development of Manduca sexta. *Insect Biochem.* **18**, 211-214.
Fichter, W. B. (1966). A theory for inflated thin-wall cylindrical beams. NASA TN D-3466 1-19.
Ghanbari, A., Rostami, A., Noorani, S. M. and Fakhrabadi, M. M. (2008). Modeling and simulation of inchworm mode locomotion. *Intelligent Robotics Appl.* **5314**, 617-624.
Greenlee, K. J. and Harrison, J. F. (2005). Respiratory changes throughout ontogeny in the tobacco hornworm caterpillar, *Manduca sexta*. *J. Exp. Biol.* **208**, 1385-1392.
Hinton, H. E. (1955). On the structure, function, and distribution of the prolegs of the Panorpoidea, with a criticism of the Berlese-Imms theory. *Trans. R. Ent. Soc. Lond.* **106**, 455-540.
Jordan, C. E. (1998). Scale effects in the kinematics and dynamics of swimming leeches. *Can. J. Zool.* **76**, 1869-1877.
Keller, J. B. and Falkovitz, M. S. (1983). Crawling of worms. *J. Theor. Biol.* **104**, 417-442.
Kier, W. M. (1992). Hydrostatic skeletons and muscular hydrostats. In *Biomechanics (Structures and Systems): A Practical Approach* (ed. A. A. Biewener), pp. 205-231. New York: Oxford University Press.
Kier, W. M. and Smith, K. K. (1985). Tongues, tentacles and trunks: the biomechanics of movement in muscular-hydrostats. *Zool. J. Linn. Soc.* **83**, 307-324.
Kramer, S. and Wigglesworth, V. B. (1950). The outer layers of the cuticle in the cockroach *Periplaneta americana* and the function of the oenocytes. *J. Cell. Sci.* **3**, 63-72.
Le Van, A. and Wielgosz, C. (2005). Bending and buckling of inflatable beams: some new theoretical results. *Thin-Walled Struct.* **43**, 1166-1187.
Lease, H. M., Wolf, B. O. and Harrison, J. F. (2006). Intraspecific variation in tracheal volume in the American locust, *Schistocerca americana*, measured by a new inert gas method. *J. Exp. Biol.* **209**, 3476-3483.
Lin, H. T. and Trimmer, B. A. (2010). The substrate as a skeleton: ground reaction forces from a soft-bodied legged animal. *J. Exp. Biol.* **213**, 1133-1142.
Lin, H. T., Dorfmann, A. L. and Trimmer, B. A. (2009). Soft-cuticle biomechanics: a constitutive model of anisotropy for caterpillar integument. *J. Theor. Biol.* **256**, 447-457.
Locke, M. (1997). Caterpillars have evolved lungs for hemocyte gas exchange. *J. Insect Physiol.* **44**, 1-20.
Mezoff, S., Papastathis, N., Takesian, A. and Trimmer, B. A. (2004). The biomechanical and neural control of hydrostatic limb movements in *Manduca sexta*. *J. Exp. Biol.* **207**, 3043-3053.
Muller, K. J., Nicholls, J. G. and Stent, G. S. (1981). *Neurobiology of the Leech*. Laurel Hollow, NY: Cold Spring Harbor Laboratory Press.
NASA (1965). Buckling of thin-walled circular cylinders. *NASA Space Vehicle Design Criteria*, NASA SP-8007.
Nelson, R. B. and Dorfmann, A. (1995). Parallel elastoplastic models of inelastic material behavior. *J. Eng. Mech.* **121**, 1089-1097.
Nijhout, H. F., Davidowitz, G. and Roff, D. A. (2006). A quantitative analysis of the mechanism that controls body size in *Manduca sexta*. *J. Biol.* **5**, 16.
Prange, H. D., Anderson, J. F. and Rahn, H. (1979). Scaling of skeletal mass to body mass in birds and mammals. *Am. Nat.* **113**, 103-122.
Quillin, K. J. (1998). Ontogenetic scaling of hydrostatic skeletons: geometric, static stress and dynamic stress scaling of the earthworm *Lumbricus terrestris*. *J. Exp. Biol.* **201**, 1871-1883.
Quillin, K. J. (1999). Kinematic scaling of locomotion by hydrostatic animals: ontogeny of peristaltic crawling by the earthworm *Lumbricus terrestris*. *J. Exp. Biol.* **202**, 661-674.
Quillin, K. J. (2000). Ontogenetic scaling of burrowing forces in the earthworm *Lumbricus terrestris*. *J. Exp. Biol.* **203**, 2757-2770.
Sawyer, R. T. (1986). *Leech Biology and Behaviour*. Oxford: Clarendon Press.
Simon, M. A., Fusillo, S. J., Colman, K. and Trimmer, B. A. (2010). Motor patterns associated with crawling in a soft-bodied arthropod. *J. Exp. Biol.* **213**, 2303-2309.
Skierczynski, B. A., Wilson, R. J. A., Kristan, W. B., Jr and Skalak, R. (1996). A model of the hydrostatic skeleton of the leech. *J. Theor. Biol.* **181**, 329-342.
Sláma, K. (1984). Recording of haemolymph pressure pulsations from the insect body surface. *J. Comp. Physiol. B* **154**, 635-643.
Sláma, K. (2003). Mechanical aspects of heartbeat reversal in pupae of *Manduca sexta*. *J. Insect Physiol.* **49**, 645-657.
Smits, A. W. (2000). Developmental changes in in vivo cardiac performance in the moth *Manduca sexta*. *J. Exp. Biol.* **203**, 369-378.
Snodgrass, R. E. (1993). *Principles of Insect Morphology*. Ithaca, NY: Cornel University Press.
Stern-Tomlinson, W., Nusbaum, M. P., Perez, L. E. and Kristan, W. B. (1986). A kinematic study of crawling behavior in the leech, *Hirudo medicinalis*. *J. Comp. Physiol. A* **158**, 593-603.
Thomas, J. C., Jiang, Z. and Wielgosz, C. (2006). Continuous and finite element methods for the vibrations of inflatable beams. *Int. J. Space Struct.* **21**, 197-222.

Trueman, E. R. (1975). *The Locomotion of Soft-Bodied Animals*. London: Edward Arnold.
Tsuchida, K. and Wells, M. A. (1988). Digestion, absorption, transport and storage of fat during the last larval stadium of *Manduca sexta*. Changes in the role of lipophorin in the delivery of dietary lipid to the fat body. *Insect Biochem.* **18**, 263-268.
Veldman, S. L., Bergsma, O. K. and Beukers, A. (2005). Bending of anisotropic inflated cylindrical beams. *Thin-Walled Struct.* **43**, 461-475.
Vogel, S. (2003). *Comparative Biomechanics*. Princeton, NJ: Princeton University Press.
Wadepuhl, M. and Beyn, W. J. (1989). Computer simulation of the hydrostatic skeleton. The physical equivalent, mathematics and application to worm-like forms. *J. Theor. Biol.* **136**, 379-402.
Wainwright, S. A. (1982). *Mechanical Design in Organisms*. Princeton, NJ: Princeton University Press.
Wainwright, S. A. (1988). *Axis and Circumference: The Cylindrical Shape of Plants and Animals*. Cambridge, MA: Harvard University Press.
Wasserthal, L. T. (1981). Oscillating haemolymph 'circulation'and discontinuous tracheal ventilation in the giant silk moth *Attacus atlas* L. *J. Comp. Physiol. B* **145**, 1-15.
Wasserthal, L. T. (1996). Interaction of circulation and tracheal ventilation in holometabolous insects. *Adv. Insect Physiol.* **26**, 297-351.
Weeks, J. C. and Truman, J. W. (1984). Neural organization of peptide-activated ecdysis behaviors during the metamorphosis of *Manduca sexta*. *J. Comp. Physiol. A* **155**, 407-422.
West, G. B., Brown, J. H. and Enquist, B. J. (1997). A general model for the origin of allometric scaling laws in biology. *Science* **276**, 122-126.
Wolfgang, W. J. and Riddiford, L. M. (1981). Cuticular morphogenesis during continuous growth of the final instar larva of a moth. *Tissue Cell* **13**, 757-772.
Wolfgang, W. J. and Riddiford, L. M. (1986). Larval cuticular morphogenesis in the tobacco hornworm, Manduca sexta and its hormonal regulation. *Dev. Biol.* **113**, 305-316.